J. Fluid Mech. (1983), *vol.* 133, *pp.* 345–376
Printed in Great Britain

Mean flow in round bubble plumes

By J. H. MILGRAM
Department of Ocean Engineering, MIT, Cambridge, MA 02139

(Received 28 January 1983)

Previous experimental studies are reviewed and those whose data are deemed reliable are identified. New experiments at larger scale are described and the results are reported. These are combined with the reliable previous studies to form a data set covering heights from 3.66 to 50 m and gasflow rates from 0.0002 to 0.59 normal m^3/s. These wide-ranging data are combined with an integral theory for bubble plumes to determine functional relationships between local plume properties and the entrainment coefficient and the fraction of the momentum flux that is carried in the turbulent velocity fluctuations. These relationships together with the integral theory provide a set of equations that are suitable for numerical solution for the mean flow properties of any round bubble plume. Examples of the numerical solutions are presented and a comparison of one of these with existing experimental data is given. The relationships between the local plume properties and the entrainment coefficient and the momentum flux carried by the turbulence are interpreted to provide a qualitative understanding of the parameters involved and their influences on the plume.

1. Introduction

When a continuous stream of gas is released in the interior of a liquid the gas takes the form of bubbles which rise owing to buoyancy and which impart a generally upward velocity to the surrounding liquid. Such bubble plumes occur above blowouts of subsea gas-containing hydrocarbon wells, and it is the desire to understand the hydrodynamics of subsea blowouts that has stimulated the most recent studies of these plumes.

Gas enters the liquid in the form of a jet, and the region through which the flow goes from jetlike to plumelike is called the zone of flow establishment. The region of the flow beneath the upper surface of the liquid extending to a depth about equal to the plume diameter is the part of the flow for which the influence of the upper surface is significant and it is called the zone of surface flow. Usually most of the vertical extent of the flow lies in the 'pure-plume' region between these two zones. It is called the zone of established flow and is the subject of this paper.

Extensive studies of single-phase plumes have taken place, and a thorough review of these is that of Chen & Rodi (1980). The fewer studies of bubble plumes that have been done show that these plumes have both notable similarities and differences with single-phase plumes. This paper extends the integral theory of plumes to include some of these differences and determines approximations for some of the needed functional relationships by analysing existing small-scale data together with new experimental data for plumes of larger scale. A review of important studies of round bubble plumes in non-stratified surroundings known to the author follows. All of the experimental studies have been for air released into water.

Kobus (1968) performed experiments on round bubble plumes in a laboratory basin having a width of 8 m and a depth of 4.7 m, with airflow rates up to 0.0058 normal m^3/s. For each airflow rate, profiles of velocity *vs.* radius were measured, and each of these was fitted with a Gaussian curve whose width and centreline velocity were chosen so as to minimize the error between the curve and the measured data. Kobus found it necessary to average his data over five-minute intervals (presumably to obtain reliable results) because the flow was 'subject to considerable fluctuations'. These fluctuations could have been caused not only by local turbulence, but also by lateral wandering motions of the plume. If wandering did occur, the long-term time-average measurements would show greater widths and smaller centreline velocities than actually existed with respect to the instantaneous locations of the wandering plume centreline; a fact which must be considered in interpreting the data.

Because the air-nozzle diameter was very small (0.2 cm in most cases), the flow in the nozzle was subsonic only for airflow rates below 0.0009 normal m^3/s. For the higher airflow rates, the supercritical flow out of the nozzle could have expanded rapidly to an unknown radius and interacted with the tank bottom so as to add an unknown amount of momentum flux to the plume. Because of this, the sonic orifice data will not be considered further here.

Subsonic-orifice Gaussian-fit centreline velocity results were given by Kobus for airflow rates of 0.00040 and 0.00057 normal m^3/s. Gaussian-fit widths were given for the 0.00040 normal m^3/s case, but not at the same set of heights as the velocity data so that interpolation between points is necessary to obtain the centreline velocity–widths pairs that are needed for the analysis here. Width data were not given for the 0.00057 normal m^3/s case, so it can only be approximated by interpolating between the 0.00040 normal m^3/s case and the next-lowest airflow for which width data are given, which is 0.0013 normal m^3/s. Owing to the uncertainty associated with these steps the Kobus data will not be included here in the primary data set used for determining plume properties. However, these data will be analysed so that they can be compared with other data.

Topham (1975) performed experiments with air bubble plumes in Saanich Inlet off Vancouver Island using air-nozzle depths up to 60 m and airflow rates up to 0.66 normal m^3/s. Profiles of flow speed *vs.* radius were measured at several heights from a horizontally suspended 12 m long beam which supported 20 vertical current meters. A 6 min average of the data from each current meter was used as the velocity at a radius equal to the distance from the beam centre to the meter. The results for plume radii and centreline velocities *vs.* height show too many deviations from smooth functions and vary in excessively irregular ways from test to test to be suitable for use here in the primary data set. Topham (private communication) has indicated that these matters are related, at least in part, to lateral motions of the beam caused by turbulence in the flow and the fact that the lateral restraint was not stiff. Nevertheless, Topham's measurements are in qualitative agreement with those of similar scale made by the author and which are described subsequently.

Fannelop & Sjoen (1980) conducted experiments in a laboratory basin having a width of 10.5 m and a depth of 10 m using airflow rates up to 0.022 normal m^3/s. Fluid velocity at various points was measured, and in order to obtain 'satisfactory repeatability' they had to average their velocity data over 10 min time intervals. Both the actual data and Gaussian curve fits to the profiles of velocity *vs.* radius are presented. The normalized standard deviation for the curve fitting is observed to be about 5%. Details of two different methods for obtaining Gaussian curve approximations and their results for these data are described by Sjoen (1982). The standard

deviation between results of the two methods is of the order of 4 %. For the subsequent analysis and comparisons considered here, the averages of the two sets of results given by Sjoen will be used.

Milgram & Van Houten (1982) performed experiments on bubble plumes in a 1.65 m diameter laboratory tank with a nozzle depth of 3.66 m at airflow rates up to 0.0022 normal m^3/s. In addition to measuring profiles of flow speed *vs.* radius at several heights, they also measured profiles of momentum flux and of gas fraction. Observations and measurements of the plumes in the tank showed that plume wandering was sufficient to bias measurements taken as long-term time averages. This difficulty was overcome by the following procedure. When a measurement was to be made at a particular height and radius, three identical measurement transducers were located on a horizontal circle of this radius and concentric with the axis of the tank. The output from each transducer was low-pass filtered with a 5 sec time constant. The resultant signals were processed by an analog-to-digital converter and a digital computer whose program discarded all data except those for which all three signals were equal to within a small fraction of the average signal level. This procedure limited retained data to those for which the plume centreline was nearly centred in the tank, so the radius from the instantaneous centreline to the instrument was known. These centering events occurred about once every five minutes on the average. For each transducer location circle, the experiment was continued until eight centring events occurred and the eight measurements were averaged together to obtain the required data point. Profiles of flow speed, momentum flux and gas fraction were fitted with Gaussian curves, with the standard deviation of the fits averaging about 3 % of the centreline values.

All current mean-flow theories for bubble plumes are integral theories for which the general forms for radial distributions of velocity and density defect (and the momentum flux by implication) are presumed to be known in advance. The presumed general forms are chosen to agree with experimental findings. Gaussian forms are most commonly used, with the mean velocity and mean density defect given by

$$u(r,z) = U(z)\,\mathrm{e}^{-r^2/b^2}, \tag{1.1}$$

$$\rho_{\mathrm{w}} - \rho_{\mathrm{p}}(r,z) = S(z)\,\mathrm{e}^{-r^2/\lambda^2 b^2}, \tag{1.2}$$

where u is the vertical velocity of the liquid, z is the height measured upward from the gas outlet, r is the radius, U is the centreline velocity, b is the 'plume radius', ρ_{w} is the mass density of water, ρ_{p} is the mean mass density of the plume, S is the density defect at the plume centreline, and λ is the ratio of 'gas-containing radius' to 'plume radius'.

Ditmars & Cederwall (1974) developed an integral theory for bubble plumes along the same lines as the integral theory for single-phase plumes presented by Morton, Taylor & Turner (1956). Both theories are based on an entrainment hypothesis under which the volume of surrounding liquid that is entrained into the plume per unit height is proportional to both the local centreline velocity and the plume circumference $2\pi b$, with a constant of proportionality being the entrainment coefficient α. Both theories approximate the plume density as that of the surrounding fluid when calculating the momentum flux and the water mass flux, so they contain errors that increase with increasing gas fraction. Also, both theories presume the momentum flux is that of the mean flow, so the momentum flux carried by the turbulence is neglected. Differences in the theories are that Ditmars & Cederwall allowed the gas to move more quickly than the liquid by means of a pre-specified 'slip velocity' and they included

the parameter λ, whereas it is absent in the single-phase plume theory of Morton *et al.*

Ditmars & Cederwall made some conclusions about the values of α and λ by comparing their theory to the data of Kobus (1968). However, these must be discounted, particularly those about λ, owing to the aforementioned artifacts involved with the Kobus data.

Fannelop & Sjoen (1980) determined both approximate similarity solutions and numerically integrated solutions to a set of equations that neglected the slip velocity of the gas, but otherwise were substantially the same as those used by Ditmars & Cederwall. Fannelop & Sjoen applied their theory to the conditions of their experiments to obtain a comparison between theory and experiment, and to make estimates of the entrainment coefficient α. This was done by choosing a value of α that was a constant, independent of depth, for each airflow rate such that the error between theory and experiment for plume radius b *vs.* height was minimized. They used a value of 0.6 for the gas/velocity radius ratio λ, where this was based on qualitative photographic observations of the radius of the gas-containing region. The values of α obtained in this way increased with increased gasflow rate; being 0.075 for a gasflow rate of 0.0050 normal m^3/s and increasing to 0.102 for a gasflow rate of 0.022 normal m^3/s. The comparison between theory and experiment for centreline velocity showed that the theoretical values averaged 15% greater than the experimental measurements.

Milgram & Van Houten (1982) developed a theory that included the effect of gas fraction on mass and momentum fluxes, and approximated the turbulent transport of mean momentum flux by assuming that a fixed fraction of this flux was carried by the turbulence. George, Alpert & Tamanini (1977) found that 8% of the mean momentum flux was carried by the turbulence in their single-phase thermal plumes in air. A comparison of velocity measurements and momentum flux measurements in the bubble plumes of Milgram & Van Houten showed that an average of 50% of the mean momentum flux was carried by the turbulence, and this value was used in applications of their theory. Bubble 'slip velocity' was included in the theory and, for the same reasons as are subsequently described here, a value of 0.35 m/s was used for applications. A comparison of measured radial profiles of velocity and gas fraction gave an average value of λ of 0.8, and this value was used in application of the theory. A fixed entrainment coefficient α was chosen for each gasflow rate in the same way as done by Fannelop & Sjoen. Milgram & Van Houten also found that α increased with increased gasflow rate; being 0.047 for a gasflow rate of 0.000205 normal m^3/s and increasing to 0.083 for a gas-flow rate of 0.00234 normal m^3/s. However, a curve of their values of α *vs.* gasflow rate does not continue smoothly onto a curve for the Fannelop & Sjoen data, which supports the result of dimensional reasoning that other factors in addition to the gasflow must be involved in determining the entrainment coefficient. The comparison between theory and experiment for the centreline velocity U *vs.* height for the Milgram & Van Houten study gives agreement without a systematic bias and a normalized standard deviation of about 7%. This completes the review of previous work.

In order to be able to use an integral plume theory to predict the mean velocity and density distributions in a bubble plume of arbitrary depth and gasflow rate, values for four parameters are required. These are the bubble 'slip speed' u_b, the gas/velocity radius ratio λ, the entrainment coefficient α, and the ratio of total momentum flux to the momentum flux carried by the mean flow, which is called γ. The effects of expected variations from the values of u_b and λ that will be estimated

subsequently have been found to be small by numerical tests. A major purpose of this paper is to use experimental results to establish functional relationships between plume properties and α and γ.

2. Theory

2.1. *The integral plume equations*

The integral plume theory is based on a principle of local similarity for which radial profiles of velocity have similar forms at different heights, as do the radial profiles of density defect. These quantities can then be specified by their centreline values $U(z)$ and $S(z)$, and their characteristic radii $b(z)$ and $\lambda b(z)$.

The gas is presumed to follow the isothermal expansion law, and mean pressure variations on horizontal planes are presumed to be small enough to have only negligible effects on the plume dynamics. Under these conditions, for a liquid of depth H, the gas density $\rho_g(z)$ is given by

$$\rho_g(z) = \frac{\rho_T(H_B - z)}{H_T}, \tag{2.1}$$

where ρ_T is the gas density at a pressure of one atmosphere, H_T is the atmospheric pressure head and H_B is the pressure head at the level of gas release:

$$H_B = H_T + H. \tag{2.2}$$

The integral plume equations will involve the local mean gas fraction $f(r, z)$, which is given by

$$f(r, z) = \frac{\rho_w - \rho_p(r, z)}{\rho_w - \rho_g(z)}, \tag{2.3}$$

and the local gas velocity, which will be approximated as the sum of the local liquid speed $u(r, z)$ and a constant slip velocity u_b, to approximate the effect of the rise velocity of the bubbles relative to the liquid. $q(z)$, $Q(z)$, $M(z)$ and $B(z)$, the gas volume flux, the liquid volume flux, the momentum flux and the buoyancy per unit height respectively, are expressed in terms of local properties as

$$q(z) = 2\pi \int_0^\infty [u(r, z) + u_b] f(r, z)\, r\, dr, \tag{2.4}$$

$$Q(z) = 2\pi \int_0^\infty u(r, z)\, [1 - f(r, z)]\, r\, dr, \tag{2.5}$$

$$M(z) = 2\pi\gamma \int_0^\infty \{u^2(r, z)\, \rho_w\, [1 - f(r, z)] + [u(r, z) + u_b]^2\, \rho_g(z) f(r, z)\}\, r\, dr, \tag{2.6}$$

$$B(z) = 2\pi g \int_0^\infty [\rho_w - \rho_g(z)]\, f(r, z)\, r\, dr. \tag{2.7}$$

γ is called the momentum amplification factor and $(\gamma - 1)/\gamma$ is the fraction of the mean momentum flux that is carried in the turbulence. g is the acceleration due to gravity.

Closure of the integral plume equations requires a relationship between local plume properties and the rate of increase with height of the liquid volume flux. Ditmars & Cederwall (1974), Fannelop & Sjoen (1980), and Milgram & Van Houten (1982) all used an entrainment hypothesis for the needed relationship, and this will be adopted here. It is

$$\frac{dQ}{dz} = 2\pi\alpha b(z)\, U(z), \tag{2.8}$$

where α is the entrainment coefficient. However, whereas all previous investigators considered the entrainment coefficient as a constant to be specified for any particular plume, here it will be considered to be dependent upon local plume properties.

The three integral plume equations can now be determined. The first is the conservation-of-liquid equation (2.8). The second is the conservation-of-gas equation, which can be expressed as

$$\frac{q_T H_T}{H_B - z} = q(z), \tag{2.9}$$

where q_T is the gas volume flow rate at a pressure of one atmosphere. The third equation results from equating the buoyancy per unit height to the spatial rate of change of momentum flux,

$$B(z) = \frac{dM}{dz}. \tag{2.10}$$

2.2. *Equations for Gaussian profiles of velocity and density defect*

Experimental evidence shows that the radial profiles of velocity and density defect are well approximated by Gaussian curves, so (1.1) and (1.2) will be used henceforth. For these profiles (2.4)–(2.7) become

$$q(z) = \frac{S(z)\,\pi\lambda^2 b^2(z)}{\rho_w - \rho_g(z)}\left[\frac{U(z)}{1+\lambda^2} + u_b\right], \tag{2.11}$$

$$Q(z) = \pi U(z)\, b^2(z)\left(1 - \frac{\lambda^2 S(z)}{[1+\lambda^2][\rho_w - \rho_g(z)]}\right), \tag{2.12}$$

$$M(z) = \pi b^2(z)\,\gamma\left\{U^2(z)\left[\frac{\rho_w}{2} - \frac{\lambda^2 S(z)}{1+2\lambda^2}\right] + \frac{\lambda^2 u_b \rho_g(z)\, S(z)}{\rho_w - \rho_g(z)}\left[\frac{2U(z)}{1+\lambda^2} + u_b\right]\right\}, \tag{2.13}$$

$$B(z) = \pi g \lambda^2 S(z)\, b^2(z). \tag{2.14}$$

The plume equations (2.8)–(2.10) then become

$$2\alpha U(z)\, b(z) = \frac{d}{dz} U(z)\, b^2(z)\left\{1 - \frac{\lambda^2 S(z)}{[1+\lambda^2][\rho_w + \rho_g(z)]}\right\}, \tag{2.15}$$

$$\frac{q_T H_T}{H_B - z} = \frac{\pi\lambda^2 b^2(z)\, S(z)}{\rho_w - \rho_g(z)}\left[\frac{U(z)}{1+\lambda^2} + u_b\right], \tag{2.16}$$

$$g\lambda^2 S(z)\, b^2(z) = \frac{d}{dz}\gamma b^2(z)\left\{U^2(z)\left[\frac{\rho_w}{2} - \frac{\lambda^2 S(z)}{1+2\lambda^2}\right] + \frac{\lambda^2 u_b \rho_g(z)\, S(z)}{\rho_w - \rho_g(z)}\left[\frac{2U(z)}{1+\lambda^2} + u_b\right]\right\}, \tag{2.17}$$

with $\rho_g(z)$ given by (2.1).

2.3. *Initial conditions near the bottom of the zone of established flow*

Equations (2.15)–(2.17) can be integrated upward numerically if all parameters are known and if conditions near the bottom of the zone of established flow are known so that the integration can be started. Equation (2.16) for the conservation of gas is valid, so two additional conditions are required. The precise determination of these requires unavailable information about the zone of flow establishment, but suitable approximations for most conditions can be made. The reasons for this are that over most of the extent of the plume the momentum gained in the zone of established flow dominates the momentum gained in the zone of flow establishment, and solutions to the plume equations are generally particularly stable to perturbations in initial conditions.

The momentum flux at the height z_E, where the integration is to be started, is estimated as the sum of the momentum flux coming from the gas outlet and an estimate of the buoyancy in the zone beneath this height. To minimize the error of this estimate, z_E should be chosen as low as possible so that the buoyancy beneath it is minimized. However, as the height of the gas outlet is approached there is expected to be more error in the first part of the integration due to inaccuracies in both the Gaussian approximations and the entrainment hypothesis. The best choice for z_E is the one that gives the best balance between these influences. Although this is not known exactly, a reasonable position would seem to be the greater of five gas outlet diameters D and the height of the zone of flow establishment for single-phase plumes given by Chen & Rodi (1980). This is

$$z_E = \min \left\{ \begin{matrix} 5D \\ 10u_0 \left(\frac{D}{g}\right)^{\frac{1}{2}} \left[\frac{\rho_g(0)}{\rho_w}\right]^{\frac{3}{4}} \end{matrix} \right\}, \tag{2.18}$$

where u_0 is the gas velocity at the outlet as determined from the gas volume flow rate and the area of the gas outlet.

Estimating the mean gas speed below $z = z_E$ as $\frac{1}{2}u_0$, the estimate for the momentum flux becomes

$$M(z_E) = q_T \rho_g(H)\, u_0 + \frac{2q(\frac{1}{2}z_E)}{u_0} [\rho_w - \rho_g(\tfrac{1}{2}z_E)]\, g z_E. \tag{2.19}$$

Finally, the centreline plume density defect is estimated as

$$S(z_E) = \tfrac{1}{2}\rho_w. \tag{2.20}$$

It must be emphasized that these cavalier estimates of $M(z_E)$ and $S(z_E)$ are not represented as accurate values for the top of the zone of flow establishment, but rather are reasonable values for beginning the numerical integration at $z = z_E$. Figure 1 is an example of the insensitivity of results over most of the plume of the numerical integration to reasonable variations in the initial conditions.

2.4. *Theoretical framework for analysis of velocity measurements*

The measurement data that will be used to determine the relationship between local plume properties and both the entrainment coefficient α and the momentum-flux amplification factor γ are the laboratory experiments of Fannelop & Sjoen (1980) and of Milgram & Van Houten (1982) as well as the larger-scale experiments described subsequently. All of these experiments included measurements of radial profiles of vertical velocity, but profiles of gas fraction and momentum flux were only measured in the second study. For the other experiments these quantities must be determined by application of the plume theory to the velocity measurements, and for consistency this procedure will be applied to all of the data. Application of the theory requires *a priori* specification of the bubble 'slip velocity' u_b and of the gas/velocity radius ratio λ.

Photographic measurements of bubble sizes made by the author (for air-bubble plumes in water) showed that most of the gas was carried by bubbles whose volumes ranged from 0.01 to 33 cm^3. Of these, most of the bubbles had volumes between 0.02 and 0.5 cm^3, for which Haberman & Morton (1954) found rise velocities in still water between 0.23 and 0.25 m/s. However, the larger and faster-moving bubbles have so much more volume than the smaller bubbles that the average gas slip speed exceeds 0.25 m/s. Haberman & Morton found a rise velocity of 0.45 m/s for 33 cm^3 bubbles, and the average gas speed is certainly less than this value. For the

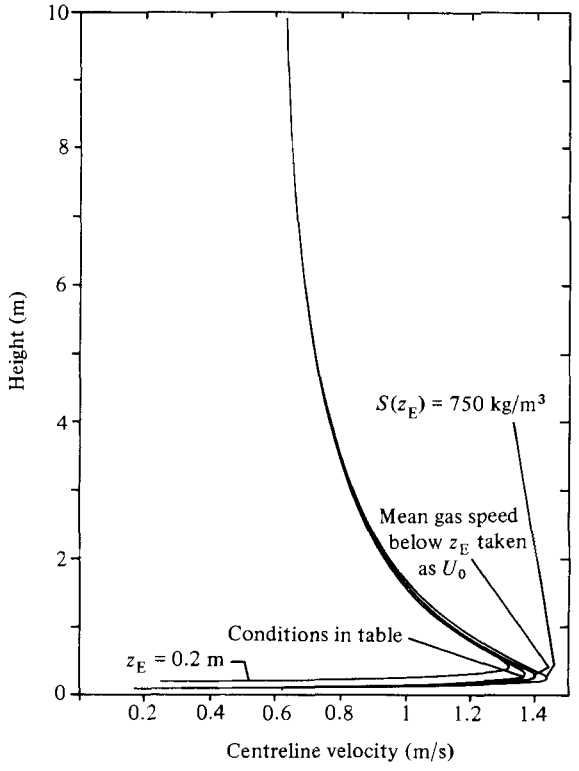

FIGURE 1. The effect of variations in initial conditions for starting the numerical integrations. Conditions are as listed below except for notations on individual curves: $H = 10$ m, $z_E = 0.1$ m, $g = 9.81$ m²/s, $q = 0.01$ normal m³/s, $S(z_E) = 500$ kg/m³, $u_0 = 25$ m/s, $\rho_T = 1.3$ kg/m³, $\rho_w = 1000$ kg/m³, $\lambda = 0.8$, $\gamma = 1.5$, $\alpha = 0.08$, $u_b = 0.35$ m/s, mean gas speed below z_E taken as $\frac{1}{2}u_0$.

subsequent application of the theory here, a value of 0.35 m/s is used. Figure 2 shows an example of the results of numerical integration of the plume equations (2.15)–(2.17) for four different values of u_b; 0, 0.30, 0.35 and 0.40 m/s. An 0.05 m/s variation in u_b changes calculated vertical velocities by about 3 %, but changing u_b from 0.35 m/s to zero changes calculated vertical velocities by about 20 %. Hence estimating u_b to within ± 0.05 m/s can be expected to give relatively accurate results, but u_b cannot be neglected altogether.

By comparing measured gas fraction profiles with measured velocity profiles, Milgram & Van Houten found an average value for λ of 0.8. No other quantitative data are available. The other plumes considered here have larger sizes and liquid velocities, but the same bubble sizes. Physical reasoning suggests that these larger plumes would have larger values of λ (although still less than 1.0). On the other hand, Fannelop & Sjoen recommend $\lambda = 0.65$. A value of 0.8 will be used here in the analysis of the measurements and this is justified, in part, by the fact that a change in λ of the order of 0.1 makes very little difference to the results. Figure 3 shows theoretical results for $\lambda = 0.8$, 0.9. The effect of the variation is seen to be very small indeed.

The Gaussian approximations given by (1.1) and (1.2) for radial profiles of velocity and density defect will be used. For each measured radial profile at a height z, $U(z)$ and $b(z)$ are determined by a fit of (1.1) to the data. The local gas density is given by (2.1) and the local gas volume flow rate is given by the left-hand side of (2.16).

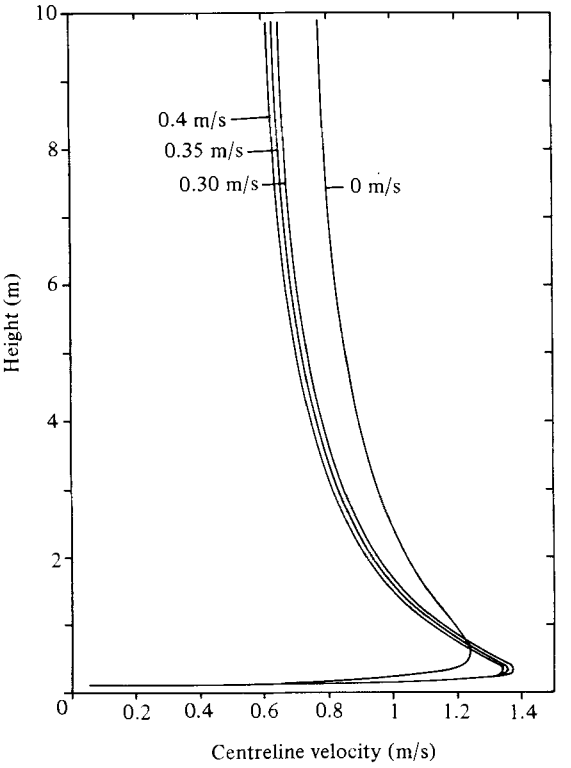

FIGURE 2. Effect of gas-bubble slip speed on solution to the plume equations. The bubble slip speeds used in the calculations are shown on each curve. Other conditions are as given in figure 1.

The local density defect can then be determined from (2.11) as

$$S(z) = \frac{[\rho_w - \rho_g(z)]\, q(z)}{\pi\lambda^2 b^2(z)\,[U(z)/(1+\lambda^2)+u_b]}. \tag{2.21}$$

The local momentum amplification factor $\gamma(z)$ will be obtained as the ratio of the total local momentum flux M_T to the momentum flux of the mean flow M_m:

$$\gamma(z) = \frac{M_T(z)}{M_m(z)}, \tag{2.22}$$

where $M_m(z)$ is obtained from (2.13) with γ set equal to 1. The total momentum flux at height z will be calculated as

$$M_T(z) = M_T(z_B) + \int_{z_B}^{z} B(z')\,dz', \tag{2.23}$$

where the buoyancy per unit height $B(z)$ is given by (2.14).

The height z_B will be taken as the lowest height in the zone of established flow at which conditions are measured or estimated. The momentum flux at z_B is estimated in the fashion of (2.19), but since z_B is generally considerably greater than z_E, a different estimate for the mean gas speed below z_B is required. Within a short distance above the height of gas release, the moving material involves a volume flux of water that is of the same order of magnitude as the volume flux of the gas. Therefore the average gas speed below z_B will be estimated as the average of $u_0\rho_g(\frac{1}{2}z_B)/\rho_w$ and

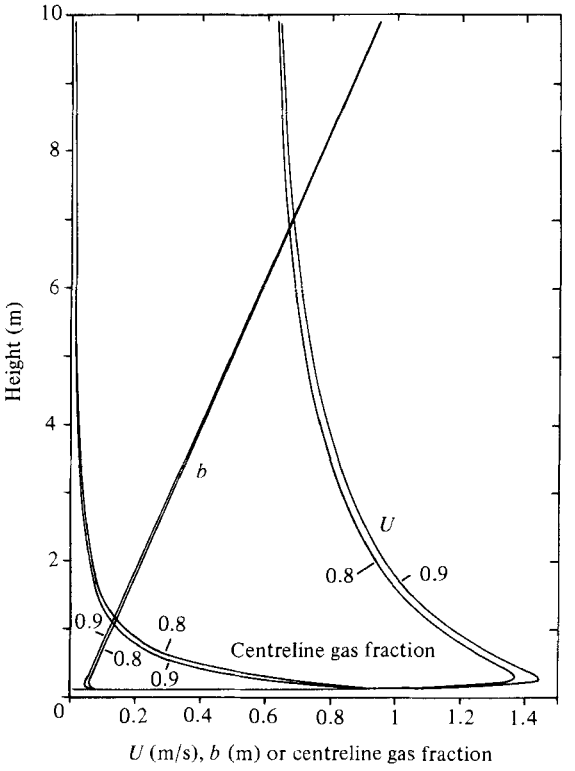

FIGURE 3. Numerical results for gas-velocity radius ratios λ of 0.8 and 0.9. The conditions for the calculations are those given in figure 1. The values for λ are shown on the curves. The difference in plume radius b for the two values of λ is almost indiscernible.

$U(z_B)+u_b$. Then

$$M_T(z_B) = q_T \rho_T u_0 + \frac{2q(\frac{1}{2}z_B) g z_B [\rho_w - \rho_g(\frac{1}{2}z_B)]}{u_0 \rho_g(\frac{1}{2}z_B)/\rho_w + U(z_B) + u_b}. \tag{2.24}$$

Because of uncertainty of the buoyancy below z_B, M_T evaluated in this way cannot be expected to be accurate enough for quantitative estimates of γ at z_B. For all measurement heights above z_B that are used, $M_T(z) \gg M_T(z_B)$, so that (2.23) is expected to be accurate enough for making quantitative estimates of γ by use of (2.22).

The other parameter that depends on local conditions to be determined from the experiments is the entrainment coefficient α. Although it could be obtained from experimental determination of the terms in (2.8), the differentiation of the liquid volume flux would accentuate experimental errors. To avoid this, α will be determined by an integration of (2.8) between heights at which radial velocity profiles are measured. Call these heights z_i ($i = 1, 2, \ldots$). Then, under the presumptions that α varies only slightly between z_i and z_{i+1} and that the liquid volume flux Q is well approximated by a linear function in this same height interval, the integral of (2.8) is solved for α as

$$\alpha\left(\frac{z_i + z_{i+1}}{2}\right) = \frac{2}{\pi} \frac{Q(z_{i+1}) - Q(z_i)}{[b(z_i) + b(z_{i+1})][U(z_i) + U(z_{i+1})][z_{i+1} - z_i]}, \tag{2.25}$$

where $Q(z)$ is given by (2.12).

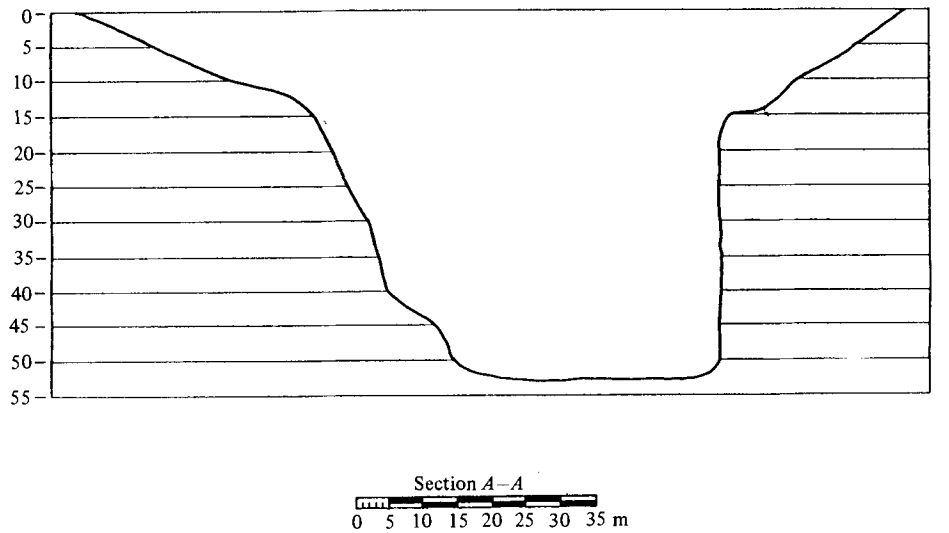

FIGURE 4. A depth profile of Bugg Spring.

3. Experiments

3.1. *Facility and equipment*

In order to increase the range of scales of bubble plume data, experiments for measuring velocity profiles were conducted with a gas-outlet depth of 50 m and gasflow rates up to 0.59 normal m^3/s. The experiments took place in Bugg Spring, which is a natural sinkhole spring located at Okahumpka, Florida, and which is part of the United States Naval Research Laboratory. Figure 4 is a cross-sectional profile of the spring. Both currents and spatial temperature variations in the spring are smaller than can be measured with ordinary instruments. A barge which is tightly moored to anchors on the shore by five cables floats on the surface with one edge of the barge over the deepest part of the spring. An existing gantry was extended to a distance of 4.6 m past this edge. A 2.5 m tall vertical air entry pipe having a 5 cm inside diameter was secured to a concrete anchor block such that the upper open end of the pipe was 50 m below the surface and vertically under the extended end of the gantry. Air was supplied to the bottom of the pipe through a hose from an airflow meter on the barge, which in turn was connected by a hose to a rotary screw air compressor on the shore.

Velocity profiles were measured with the use of a horizontal array of 36 vertical current meters configured as a cross as shown in figure 5. Each of the two arms of the cross was 12.9 m long, and the distance between adjacent current meters was 0.71 m. This permitted an accurate estimation of the location of the instantaneous centre of the plume from the location on each of the arms on the cross at which the velocity was a maximum.

A system of four support cables was used to adjust the height of the cross and to provide horizontal restraint against turbulence-induced motions of the cross. A taut upper cable attached the upper bridle shown in figure 5 to the gantry. A taut lower cable attached to the lower bridle passed through a sheave near the air outlet and then went to the barge. Two adjacent ends of the cross rode on vertical cables tensioned to about 10^4 N which led from the edge of the barge to anchor weights on the bottom.

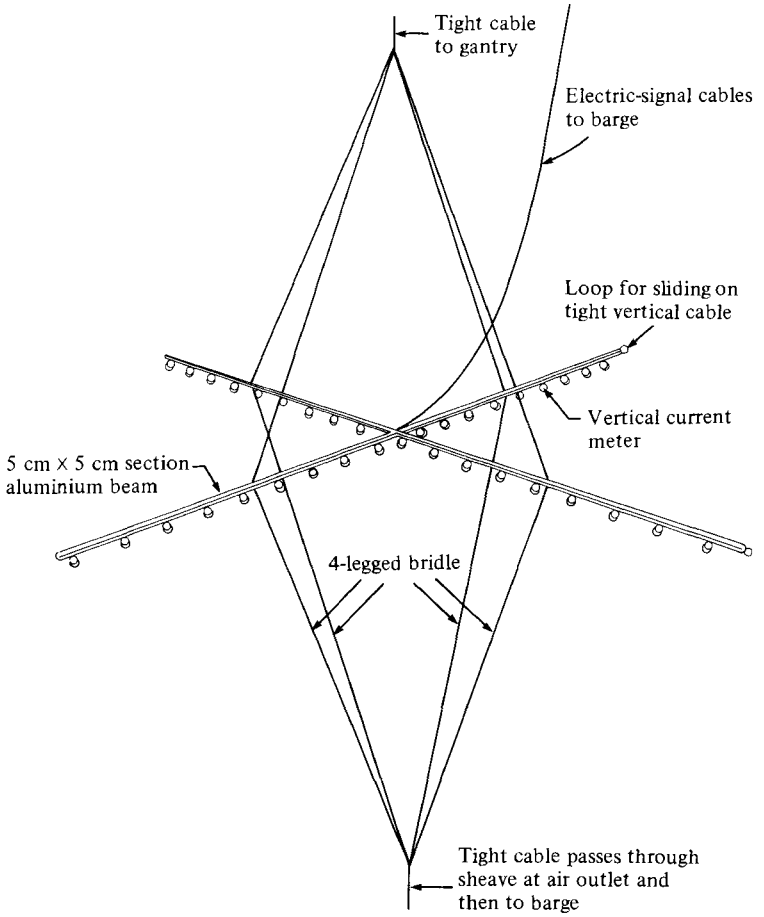

FIGURE 5. Current-meter array used for measuring radial profiles of vertical velocity.

The current meters were made from the mechanical speed-detecting parts of Aanderaa current meters and 36 electronic signal conditioners, each of which contained a low-pass filter with a 10 s time constant. The resulting signals were sampled at a rate of 1 Hz through 36 analog-to-digital channels of a digital computer for 10 min for each airflow rate and current-meter cross height. Each of the groups of 36 samples was obtained in a time interval of about 0.5 ms, so the samples can be considered to be simultaneous. Finally, for each channel each set of ten successive samples was averaged together, giving 60 of these short-time averaged measurements for each of the 36 channels in a 10 min measurement period. These measurements were made for airflow rates of 0.024, 0.118, 0.283 and 0.590 normal m^3/s; and for heights above the air outlet of 16.47, 25.62, 37.81, 43.90 and 46.95 m.

3.2. *Data reduction*

The purpose of the data reduction was to fit a Gaussian function as given in (1.1) to every radial profile measured with respect to the instantaneous location of the plume centreline and thereby obtain values for the centreline velocity U and the plume radius b. This was done by the following steps.

(1) For each 36-point, 10 s velocity average, there were 18 values along one axis of the measuring cross and 18 values along the other. Spline cubic interpolating functions were fitted to each of these 18 sets of points. The location of the maximum

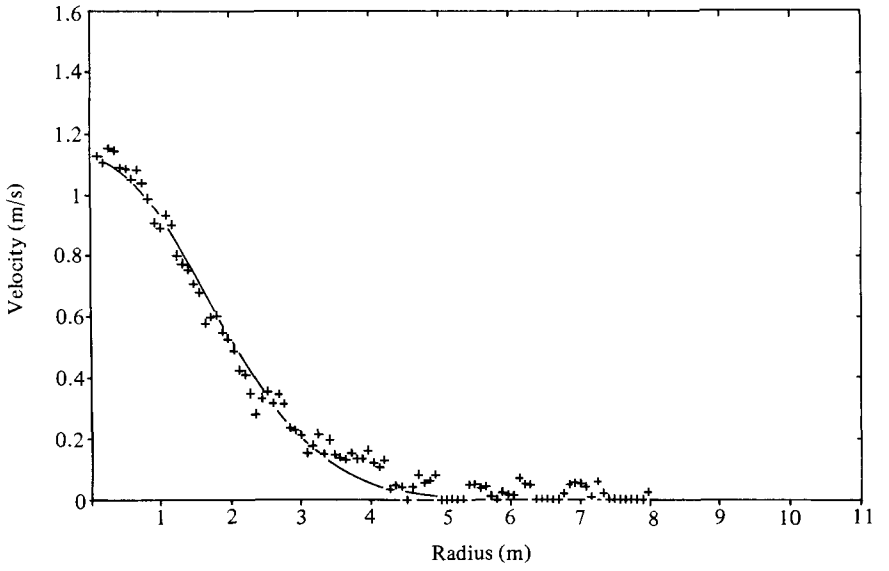

FIGURE 6. An example of reduced data for a radial profile of vertical velocity. The case shown is for a gasflow rate of 0.283 normal m^3/s and a height of 16.47 m above the gas outlet. +, reduced data point; ——, Gaussian-function fit to the data.

of each of these functions was taken as the value in 'cross coordinates' for the location of the plume centre. The distance from this location to each of the current meters was determined so that 36 sets of values (u, r) were obtained. This was done for all 60 sets of 10 s averages so that 2160 pairs of (u, r)-values were obtained for each airflow rate and measurement height.

(2) The range of values of radius r was partitioned into segments 0.08 m long. The values of u for all the r-values falling in any particular segment were averaged together to obtain a value of u for the midpoint of the segment. This reduced the number of pairs of (u, r)-values for each airflow rate and measurement height to about 100. Figure 6 shows an example of a plot of these values.

(3) A Gaussian function of the form of (1.1) was fitted to the reduced data points with U and b chosen to minimize the standard deviation between the function and the points. Figure 6 shows the Gaussian approximation to its data.

(4) The above procedure gave 20 radial profiles of velocity. The one for a measurement height of 46.95 m at an airflow rate of 0.118 normal m^3/s was 'out of line' with other profiles, and the measured profile had excessive scatter. Therefore this profile was eliminated from the data, leaving 19 of these larger-scale profiles available for analysis.

(5) The current meters measured velocities in the (r, z)-plane. Since the radial mean velocities are small in comparison with the vertical mean velocities, their effects on the measured mean velocities are small. However, a small correction can be, and was, made for this. For each airflow rate the values of $b(z)$ and $U(z)$ were fitted by spline cubic functions so that their derivatives could be easily evaluated. Then, using the form of (1.1) and a radial integration of the continuity equation (div $V = 0$, neglecting here the effects of the variation in mean density) the small radial velocity was found. From this and the measured velocities in the (r, z)-plane, the vertical velocity components were calculated. These radial profiles of vertical velocity were then fitted with Gaussian curves as before. The results are shown in table 1.

	Raw		Smooth						Airflow (normal
z	b	U	b	U	q	Q	S	γ	m³/s)
				Bugg Spring experiment data					
1.98	0.162	1.129	0.150	1.127	0.0042	0.077	88.21	—	
16.47	1.540	0.489	1.572	0.506	0.0055	3.929	1.68	1.24	
25.82	1.920	0.515	1.967	0.477	0.0070	5.797	1.40	1.50	0.024
37.81	2.822	0.498	2.466	0.562	0.0109	10.725	1.28	1.16	
43.90	2.470	0.608	2.895	0.553	0.0149	14.555	1.29	1.15	
46.95	2.980	0.538	3.191	0.516	0.0184	16.503	1.35	1.26	
1.98	0.250	1.543	0.257	1.542	0.0204	0.306	118.20	—	
16.47	1.780	0.860	1.732	0.863	0.0272	8.124	5.12	1.23	
25.62	2.399	0.829	2.476	0.823	0.0345	15.834	3.27	1.14	0.118
37.81	3.686	0.833	3.621	0.838	0.0534	34.475	2.34	0.91	
43.90	4.355	0.745	4.384	0.743	0.0735	44.811	2.36	1.07	
1.98	0.338	1.739	0.328	1.740	0.0490	0.552	159.24	—	
16.47	2.320	1.114	2.359	1.109	0.0653	19.351	5.65	0.85	
25.62	3.590	0.970	3.583	0.971	0.0827	39.102	3.39	0.83	0.283
37.81	5.569	0.881	5.365	0.906	0.1280	81.840	2.44	0.77	
43.90	5.976	0.912	6.393	0.861	0.1762	110.436	2.45	0.81	
46.95	7.190	0.794	6.955	0.823	0.2172	124.919	2.62	0.88	
1.98	0.395	2.103	0.412	2.105	0.1022	1.041	182.09		
16.47	2.609	1.326	2.488	1.316	0.1362	25.493	9.44	0.99	
25.62	3.399	1.174	3.615	1.188	0.1723	48.652	6.08	0.99	0.590
37.81	5.556	1.189	5.296	1.184	0.2668	104.145	4.40	0.83	
43.90	6.108	1.171	6.343	1.162	0.3674	146.677	4.28	0.81	
46.95	7.030	1.121	6.944	1.129	0.4527	170.688	4.49	0.84	
				Fannelop & Sjoen data					
0.65	0.110	0.985	0.113	0.987	0.0026	0.038	106.55	—	
2.25	0.300	0.750	0.293	0.748	0.0028	0.200	20.41	1.06	
3.85	0.465	0.630	0.465	0.620	0.0031	0.420	9.83	1.08	0.005
5.45	0.600	0.545	0.614	0.569	0.0035	0.672	6.55	1.11	
7.05	0.735	0.585	0.721	0.566	0.0039	0.922	5.35	1.13	
8.65	0.765	0.575	0.769	0.580	0.0044	1.076	5.30	1.25	
0.65	0.135	0.975	0.134	0.978	0.0052	0.052	152.73	—	
2.25	0.310	0.900	0.307	0.893	0.0057	0.260	33.51	1.30	
3.85	0.465	0.815	0.491	0.815	0.0062	0.614	15.18	1.03	0.010
5.45	0.710	0.735	0.665	0.749	0.0069	1.036	9.65	0.99	
7.05	0.775	0.710	0.807	0.696	0.0078	1.420	7.67	1.07	
8.65	0.905	0.655	0.897	0.659	0.0089	1.660	7.31	1.28	
0.65	0.135	1.130	0.134	1.131	0.0078	0.059	206.48	—	
2.25	0.355	1.050	0.362	1.049	0.0085	0.426	32.63	0.91	
3.85	0.540	0.975	0.518	0.974	0.0094	0.816	18.33	0.88	0.015
5.45	0.615	0.900	0.645	0.904	0.0104	1.174	13.79	0.97	
7.05	0.800	0.840	0.781	0.836	0.0117	1.596	11.06	1.07	
8.65	0.965	0.765	0.970	0.766	0.0133	2.255	8.63	1.09	
0.65	0.155	1.170	0.161	1.162	0.0115	0.086	209.19	—	
2.25	0.350	1.055	0.334	1.077	0.0126	0.369	55.53	1.47	
3.85	0.515	1.020	0.524	1.008	0.0138	0.860	25.88	1.15	0.0221
5.45	0.705	0.965	0.720	0.945	0.0153	1.529	15.85	1.02	
7.05	0.930	0.855	0.911	0.881	0.0172	2.286	11.62	1.01	
8.65	1.080	0.815	1.086	0.807	0.0197	2.978	9.83	1.13	

z	Raw b	Raw U	Smooth b	Smooth U	q	Q	S	γ	Airflow (normal m³/s)
				Milgram & Van Houten data					
0.32	0.025	0.662	0.024	0.664	0.0002	0.001	168.73	—	
0.96	0.063	0.438	0.064	0.432	0.0002	0.006	31.50	2.10	
1.58	0.103	0.321	0.101	0.331	0.0002	0.011	15.03	2.45	0.00021
2.20	0.128	0.326	0.129	0.319	0.0002	0.017	9.76	2.32	
2.78	0.144	0.358	0.144	0.360	0.0002	0.023	7.95	1.93	
0.32	0.031	0.774	0.030	0.772	0.0004	0.002	244.43	—	
0.96	0.082	0.527	0.085	0.537	0.0004	0.012	40.01	1.74	
1.58	0.129	0.456	0.125	0.441	0.0004	0.021	21.40	2.00	0.00050
2.20	0.158	0.416	0.161	0.426	0.0004	0.034	13.72	1.85	
2.78	0.201	0.445	0.200	0.442	0.0005	0.056	9.17	1.44	
0.32	0.039	0.903	0.039	0.896	0.0009	0.004	312.58	—	
0.96	0.100	0.598	0.099	0.628	0.0009	0.019	63.62	2.02	
1.58	0.137	0.553	0.138	0.507	0.0010	0.030	38.18	2.66	0.00118
2.20	0.183	0.446	0.182	0.478	0.0010	0.049	23.83	2.51	
2.78	0.248	0.498	0.248	0.490	0.0011	0.094	13.41	1.69	
0.32	0.048	1.021	0.048	1.017	0.0018	0.006	387.81	—	
0.96	0.117	0.675	0.116	0.691	0.0018	0.028	87.76	2.28	
1.58	0.167	0.594	0.168	0.569	0.0019	0.050	48.91	2.70	0.00234
2.20	0.223	0.539	0.222	0.556	0.0020	0.085	29.94	2.35	
2.78	0.288	0.580	0.288	0.575	0.0022	0.149	18.43	1.70	

TABLE 1. The momentum-amplification factors and plume properties obtained from the data analysis at the measurement heights

4. Data analysis

4.1. *The data set*

The goals of the data analysis are the determinations and explanations of functional relationships between local plume properties and the entrainment coefficients α and the momentum amplification factor γ. The experimental measurements used for these are the relatively small-scale measurements of Milgram & Van Houten (1982), the measurements at about three times larger scale of Fannelop & Sjoen (1980) and the measurements at about fifteen times larger scale made in Bugg Spring. Each of these sets of measurements contains several radial profiles of vertical velocity at each of several airflow rates, with these profiles approximated by Gaussian functions of the form of (1.1). Thus the data to be used here are in the form of values $b(z)$ and $U(z)$ at each airflow rate.

For the Fannelop & Sjoen experiments the lowest measurement height was 6.5% of the gas-outlet depth, whereas for the Milgram & Van Houten experiments and for the Bugg Spring experiments the equivalent percentages were 26% and 32% respectively. The percentage is small enough for (2.24) to be applied at the lowest height for the Fannelop & Sjoen experiments, but this is not the case for the two latter experiments. In these cases, conditions at adequately low points were estimated by an application of the integral theory. This was done as follows. For each airflow rate, the plume equations (2.15)–(2.17) were numerically integrated several times starting at a height z_E as given by (2.18); each time with different values of α and γ, which were taken, for this step only, to be independent of height. The integration that best

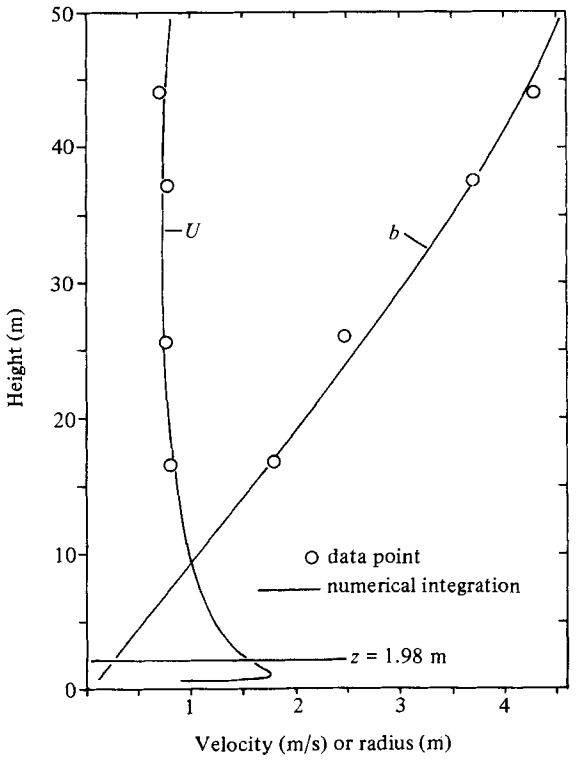

FIGURE 7. Example of a numerical integration used to estimate conditions at a low point in the zone of established flow. The conditions of the example correspond to an airflow rate of 0.118 normal m^3/s in the Bugg Spring experiments. The numerical integration was done with $\lambda = 0.8$, $z_E = 0.5$ m and $S(z_E) = 500$ kg/m^3. The best fit to the data was with $\gamma = 1.1$ and $\alpha = 0.087$, which is the case that is shown.

fitted the measured values of $b(z)$ and $U(z)$ was chosen in each case. An example of this is shown in figure 7. As is demonstrated in figure 1, errors in initial conditions for beginning the integration are most influential in the region below the minimum (maximum negative) slope of the function $U(z)$. Therefore a value of z_B was chosen for application of (2.24) that was above this point of minimum slope, and the required values of $U(z_B)$ and $b(z_B)$ were obtained from the numerical integration. The values used for z_B were 0.32 m for the Milgram & Van Houten experiments and 1.98 m for the Bugg Spring experiments.

For all three sets of experiments, values of $b(z)$ and $U(z)$ were fitted with spline cubic functions. Instead of forcing these functions to fit all the data points exactly, functions with four equally spaced nodal points with extrapolated end point curvatures were used subject to the criterion of minimum variance with the unsmoothed data. Since data at five or six heights were used, this process introduced a small amount of data smoothing. The spline cubic functions were used for the remainder of the data analysis. Table 1 shows both the unsmoothed data and the evaluations of the spline cubic functions. At each data height these evaluations were used together with (2.21) and (2.14) to determine the centreline density defect and the buoyancy per unit height which was then in turn fitted with a four-nodal-point cubic spline function. This was then integrated by quadrature to evaluate (2.23) at each data height. With this done, the momentum amplification factor was evaluated from (2.22) at each data height except for z_B, and these values are also shown

in table 1. Finally, table 1 shows the values of the liquid volume flux $Q(z)$ which were determined from (2.12).

The values of the entrainment coefficient α were determined from (2.25) at positions midway between data heights, and these are shown in table 2. Values of both α and γ for the highest measurement point at the two largest gasflow rates in the Milgram & Van Houten data appear 'out of line' with other values. Therefore these two data rows for both the α- and γ-data are not used in the subsequent data analysis. They are shown in tables 1 and 2 because they were used in the raw data set.

4.2. *The entrainment coefficient*

For single-phase plumes many investigators have proposed a constant value for the entrainment coefficient, while others (cf. Fox 1974; Seban & Behnia 1976) have suggested a functional relationship between local plume properties and the entrainment coefficient of the form,

$$\alpha_{\text{single phase}} = K_1 + \frac{K_2}{F_r^2} \tag{4.1}$$

where K_1 and K_2 are constants and the densiometric plume radius Froude number is given in terms of the variables used here as

$$F_r = U\left(\frac{\rho_w}{gbS}\right)^{\frac{1}{2}}. \tag{4.2}$$

The entrainment coefficients for bubble plumes in the data set are not constants, and a quantitative comparison with (4.1) shows that this functional relationship does not apply to bubble plumes. Therefore the approach taken here is to first determine the dimensionless group upon which the entrainment coefficient is most dependent and then to determine an empirical relationship between the group and the entrainment coefficient, based on the measured data and a few simple concepts. The purposes of this approach are to provide a quantitative formula for predicting entrainment coefficients and to aid in achieving a qualitative physical understanding of how the bubbles influence entrainment.

It is assumed that the viscous forces are small in comparison with pressure, inertia and surface-tension forces. Then the local independent variables are b, g, S, $\rho_w - \rho_g$, u_b, T, and U or q. Either U or q can be taken as independent, but not both. The relationship between the entrainment coefficient and each dimensionless grouping of these variables with rational exponents whose denominators were 10 or less was examined and the one giving the best collapse of the data is $\Delta^{\frac{1}{5}} q^{\frac{2}{5}} g^{\frac{3}{10}} (\rho_w - \rho_g)^{\frac{1}{2}} T^{-\frac{1}{2}}$, where the centreline gas fraction is

$$\Delta = \frac{S}{\rho_w - \rho_g}. \tag{4.3}$$

This dimensionless group will be called the bubble Froude number F_B, and it will be helpful to express it as

$$F_B = \Delta^{\frac{2}{5}} \frac{L_m}{L_D}, \tag{4.4}$$

where

$$L_m = \left(\frac{q^2}{g\Delta^2}\right)^{\frac{1}{5}}, \tag{4.5}$$

$$L_D = \frac{[T/g(\rho_w - \rho_g)]^{\frac{1}{2}}}{\Delta^{\frac{1}{5}}}. \tag{4.6}$$

L_m is a measure of the mixing distance of bubble motions in the turbulence, as will

z	b	U	q	S	W	α	Airflow (normal m^3/s)
			Bugg Spring experiment data				
9.23	0.86	0.817	0.0047	44.95	0.290	0.060	
21.05	1.77	0.492	0.0062	1.54	0.183	0.037	
31.71	2.22	0.520	0.0085	1.34	0.244	0.056	0.024
40.86	2.68	0.557	0.0126	1.28	0.122	0.067	
45.43	3.04	0.535	0.0165	1.32	0.061	0.063	
9.23	0.99	1.203	0.0234	61.66	0.290	0.072	
21.05	2.10	0.843	0.0304	4.19	0.183	0.076	0.118
31.71	3.05	0.831	0.0419	2.81	0.244	0.096	
40.86	4.00	0.790	0.0618	2.35	0.122	0.085	
9.23	1.34	1.425	0.0560	82.45	0.290	0.108	
21.05	2.97	1.040	0.0730	4.52	0.183	0.111	
31.71	4.47	0.938	0.1004	2.91	0.244	0.133	0.283
40.86	5.88	0.883	0.1483	2.44	0.122	0.144	
45.43	6.67	0.842	0.1946	2.53	0.061	0.135	
9.23	1.45	1.710	0.1168	95.77	0.290	0.108	
21.05	3.05	1.252	0.1521	7.76	0.183	0.106	
31.71	4.46	1.186	0.2094	5.24	0.244	0.137	0.590
40.86	5.82	1.173	0.3091	4.34	0.122	0.163	
45.43	6.64	1.146	0.4056	4.39	0.061	0.165	
			Fannelop and Sjoen data				
1.45	0.20	0.868	0.0027	63.48	0.162	0.092	
3.05	0.38	0.684	0.0030	15.12	0.162	0.084	
4.65	0.54	0.594	0.0033	8.19	0.162	0.078	0.005
6.25	0.67	0.568	0.0037	5.95	0.162	0.066	
7.85	0.75	0.573	0.0041	5.33	0.162	0.036	
1.45	0.22	0.935	0.0054	93.12	0.162	0.101	
3.05	0.40	0.854	0.0060	24.34	0.162	0.103	
4.65	0.58	0.782	0.0066	12.42	0.162	0.093	0.010
6.25	0.74	0.722	0.0073	8.66	0.162	0.072	
7.85	0.85	0.678	0.0083	7.49	0.162	0.041	
1.45	0.25	1.090	0.0082	119.56	0.162	0.135	
3.05	0.44	1.011	0.0089	25.48	0.162	0.087	
4.65	0.58	0.939	0.0099	16.06	0.162	0.065	0.015
6.25	0.71	0.870	0.0110	12.42	0.162	0.068	
7.85	0.88	0.801	0.0125	9.84	0.162	0.093	
1.45	0.25	1.120	0.0120	132.36	0.162	0.102	
3.05	0.43	1.042	0.0131	40.71	0.162	0.109	
4.65	0.62	0.976	0.0145	20.87	0.162	0.110	0.0221
6.25	0.82	0.913	0.0162	13.73	0.162	0.101	
7.85	1.00	0.844	0.0184	10.72	0.162	0.082	
			Milgram and Van Houten data				
0.64	0.04	0.548	0.0002	100.11	0.175	0.045	
1.27	0.08	0.381	0.0002	23.27	0.169	0.040	0.00021
1.89	0.12	0.325	0.0002	12.39	0.169	0.043	
2.49	0.14	0.340	0.0002	8.85	0.158	0.039	
0.64	0.06	0.654	0.0004	142.22	0.175	0.065	
1.27	0.10	0.489	0.0004	30.70	0.169	0.047	0.00050
1.89	0.14	0.434	0.0004	17.56	0.169	0.055	
2.49	0.18	0.434	0.0004	11.44	0.158	0.074	

z	b	U	q	S	W	α	Airflow (normal m³/s)
0.64	0.07	0.762	0.0009	188.10	0.175	0.071	0.00118
1.27	0.12	0.568	0.0010	50.90	0.169	0.042	
1.89	0.16	0.493	0.0010	31.01	0.169	0.063	
2.49	0.22	0.484	0.0011	18.62	0.158	0.118	
0.64	0.08	0.854	0.0018	237.78	0.175	0.078	0.00234
1.27	0.14	0.630	0.0019	68.33	0.169	0.060	
1.89	0.19	0.563	0.0020	39.43	0.169	0.083	
2.49	0.25	0.566	0.0021	24.19	0.158	0.121	

TABLE 2. The entrainment coefficients and plume properties at heights midway between measurement heights. The entrainment coefficients have been evaluated by (2.25) and the properties b, U, q and S are the averages of the values above and below the midpoints. W is the distance $z_{i+1}-z_i$ used in (2.25) divided by the total plume height.

be explained shortly. L_D is the characteristic distance between bubbles since $(T/g(\rho_w-\rho_g))^{\frac{1}{2}}$ is the characteristic lengthscale of a bubble. Application of the experimentally determined equation (11) of Hu & Kintner (1955), for the maximum stable drop diameter of a liquid in another of different density, to the case of a gas bubble in water gives a mean diameter of $3.77(T/g(\rho_w-\rho_g))^{\frac{1}{2}}$. This is the diameter of a spherical bubble having the same volume as the moving non-spherical bubble. For air bubbles in water this volume is 0.8 cm³, which is consistent with the typical sizes that are observed.

Figure 8 shows the data points of α *vs.* F_B. In addition to the data points, an additional condition used in determining a form for a functional relationship between α and F_B is that as $F_B \to \infty$ the plume is expected to act like a single-phase plume because each bubble is mixed through a volume that contains many other bubbles so that the bubbles and their wakes are diffuse. For this limit the entrainment coefficient relationship will be required to approach (4.1). A functional relationship that meets these conditions and which is consistent with the trend of the data in figure 8 is

$$\alpha(F_B, F_r) = \frac{F_B^{A_1}}{(A_2+F_B)^{A_1}}\left\{K_1+\frac{K_2}{F_r^2}\right\}. \tag{4.7}$$

For fitting (4.7) to the data in table 2 each datum point α_j was assigned a weight W_j taken as the ratio of the vertical distance $z_{i+1}-z_i$ used in (2.25) for evaluating α_j to the total depth H. The constants A_1, A_2, K_1 and K_2 were chosen so as to minimize the weighted square error E_α^2 over the 53 data points of table 2 that were used:

$$E_\alpha^2 = \sum_{j=1}^{53} W_j[\alpha_j-\alpha(F_B, F_r)]^2. \tag{4.8}$$

The value of K_2 found by this process was so small that, over the range of data points, the K_2 term in (4.7) varied from 2% to 6% of the K_1 term. The value found for A_1 was 0.95. Because of these findings and the fact that the data are neither comprehensive enough or accurate enough to predict α in complete detail, it was deemed appropriate to set K_2 to zero and A_1 to 1 and thereby replace (4.7) with the simpler form

$$\alpha(F_B) = K\frac{F_B}{A+F_B}. \tag{4.9}$$

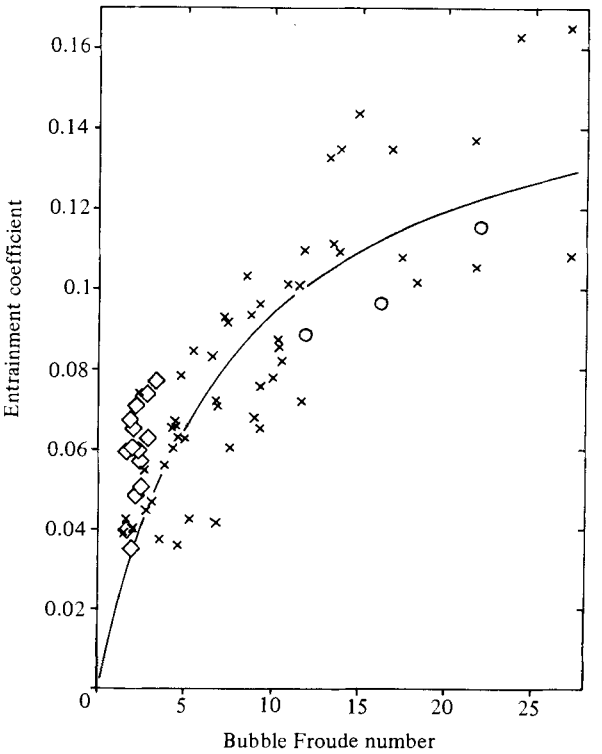

FIGURE 8. The entrainment coefficient α *vs.* the bubble Froude number F_B: ×, calculated from primary data set; ◇, calculated from subsonic-orifice Kobus data; ○, average of calculated values from Topham data: the points shown from left to right are for gas-outlet depths of 60, 60 and 53 m and gasflow rates of 0.367, 0.443 and 0.660 normal m^3/s respectively, ——, equation (4.9) with $K = 0.165$ and $A = 7.598$.

The weighted error-minimization process was then repeated, with the results

$$K = 0.165, \quad A = 7.598. \tag{4.10a, b}$$

Figure 8 shows the function $\alpha(F_B)$.

Much of the scatter of the data points in figure 8 has been found to result from small variations from smooth functions in the measured values of b *vs.* z. This scatter can be greatly reduced by a consideration of averages over height. For each experiment at a fixed airflow rate, the bubble Froude numbers at different heights vary by up to 25 % from their height average as a rule. This variation is small enough to allow a comparison of height-averaged entrainment coefficient with height-averaged bubble Froude number to be useful. In forming these height averages, the individual quantities were weighted in accordance with the values of W given in table 2. Figure 9 shows the height-averaged data points. A function of the form of equation (4.9) was fitted to these data and the best (minimum r.m.s. error) fit was obtained with $K = 0.165$ and $A = 7.907$. Figure 9 shows both this function and the previous fit to the individual data points with $A = 7.598$. The fact that the difference is so small means that the influence of the scatter on the functional fit can be neglected, so the values given in (4.10) will be used in subsequent sample calculations.

The process of entrainment across an interface between rotational and irrotational fluids is explained in detail by Townsend (1976, chap. 6). Two aspects of the entrainment process that are identified are

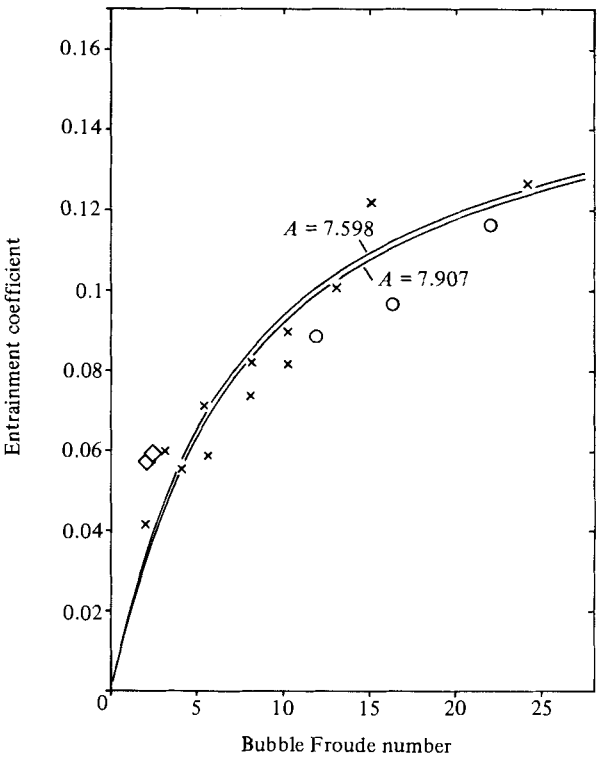

FIGURE 9. Entrainment coefficient *vs.* bubble Froude number for height-averaged data: ×, calculated from primary data set; ◇, calculated from subsonic-orifice Kobus data; ○, calculated from Topham data; ——, equation (4.9) with $K = 0.165$ and A as shown.

(1) the entrainment by ordinary turbulent eddies of the rotational motion at the interface;

(2) the increase of entraining interface area caused by undulations and folding of the interface. In the case of free turbulent shear flows this effect is made particularly strong by 'entrainment eddies', which grow due to interfacial instabilities and ultimately overturn and engulf parcels of formerly irrotational fluid in the rotational domain.

The increase in entrainment coefficient with increasing bubble Froude number can be qualitatively understood, at least in part, in terms of these effects.

George *et al.* (1977) measured higher r.m.s. turbulence levels in the centre of a single-phase plume than at larger radii. This can be expected to occur for bubble plumes as well. Because the bubbles and their wakes generally move faster than the surrounding water, they can mix the more turbulent central fluid towards the edges of the plume. The effectiveness of carrying out this mixing all the way to the entrainment interface must be increased when the mixing distance of each bubble is increased with respect to the bubble spacing by increasing the lateral mixing action from bubble to bubble. In addition, the mixing action of the bubbles can mix the high-velocity fluid near the centre of the plume towards the edges. To the extent that this process is unsteady it increases the turbulence level near the entrainment interface. Both of these effects increase the turbulent energy of the ordinary eddies near the interface.

Townsend (1976, §6.14) presents similarity arguments which indicate that the

augmentation of the entrainment coefficient by the 'entrainment eddies' is proportional to the ratio of the r.m.s. turbulent velocity to the mean centreline velocity. Although the analysis is for a two-dimensional flow, the arguments apply to axisymmetric flows as well just so long as there are instabilities that start the entrainment eddies. These undeniably do form, as they can be seen as billows along the sides of the plume (see the photograph presented by Fannelop & Sjoen 1980). Therefore the increase in turbulence near the interface associated with increased bubble Froude number is expected to increase the entrainment coefficient through action of the entrainment eddies in addition to the direct increase associated with the ordinary eddies.

The characteristic length $L_m = (q^2/g\Delta^2)^{\frac{1}{5}}$ has been interpreted here as the bubble mixing distance. By combining (2.11) and (4.5) this can be written as

$$L_m = \pi^{\frac{2}{5}}\left[\left(\frac{U}{1+\lambda^2}+u_b\right)^2/g\right]^{\frac{1}{5}}(\lambda b)^{\frac{4}{5}}.$$

Thus on a logarithmic scale the radius of the gas-containing region contributes 80 % to the mixing distance and $(U/(1+\lambda^2)+u_b)^2/g$ contributes 20 %. This latter characteristic length is a measure of how far a bubble can penetrate against the hydrostatic pressure, because the quantity in parentheses is the average bubble speed in the gas-containing region and the added water mass of a bubble is proportional to the volume of the bubble. The factor of $\Delta^{\frac{2}{5}}$ in the definition of the bubble Froude number can be viewed as a modification to the ratio L_m/L_D to account for the effect of the bubble size on the mixing process.

4.3. *The momentum-amplification factor*

A similar process to the one used for the entrainment coefficient was used to find an empirical function for the momentum-amplification factor γ. The dimensionless grouping of the independent variables giving the best collapse of the data of table 1 is $U^2(\rho_w-\rho_g)^{\frac{1}{2}}g^{-\frac{1}{2}}\Delta^{-\frac{3}{2}}T^{-\frac{1}{2}}$. This quantity will be called the phase distribution number N_P, and it can be expressed as

$$N_P = L_V/L_D, \tag{4.11}$$

where L_V is the vertical lengthscale of the plume motion:

$$L_V = U^2/g\Delta. \tag{4.12}$$

For a fixed value of λ, L_V is a measure of the vertical distance over which the momentum flux is significantly altered by buoyancy, since the momentum flux is very nearly doubled in a distance of $L_V/2\lambda^2$. The vertical distance L_V in units of the characteristic distance between bubbles is N_P. Figure 10 shows the data points of γ *vs.* N_P. For determining the form of a functional relationship between γ and N_P two conditions were used in addition to the data points. These are as follows.

(1) As $N_P \to 0$ the plume degenerates to an occasional single bubble. In this limit, γ, the ratio of total momentum flux to the momentum flux in the mean flow becomes large without limit.

(2) As $N_P \to \infty$ the bubbles are very closely spaced and the plume must act like a single-phase plume. Most single-phase plume investigations have been based on $\gamma = 1$, although the measurements of George *et al.* (1977) indicate $\gamma = 1.07$. Data fits for both asymptotic limits were determined.

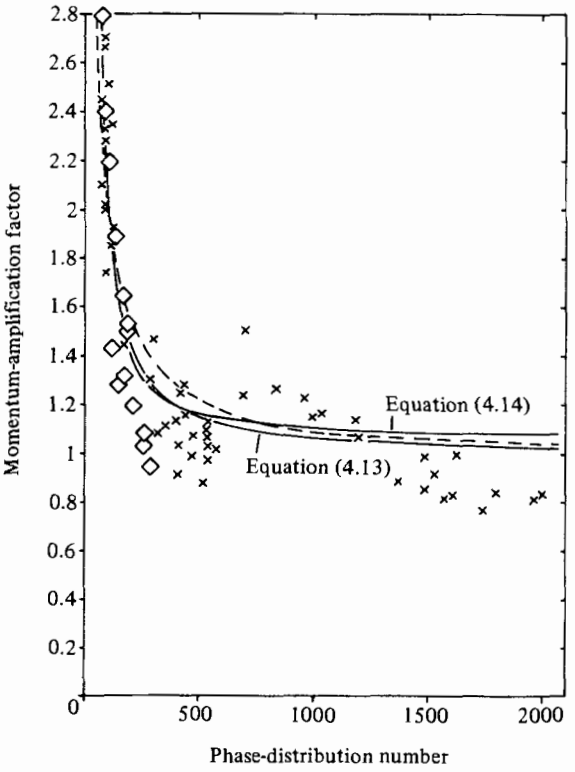

FIGURE 10. The momentum-amplification factor γ *vs.* the phase-distribution number N_P. ×, calculated from primary data set; ◇, calculated from subsonic-orifice Kobus data; ——, equation (4.13) with $C_1 = 377.7$ and $C_2 = 1.25$, and (4.14) with $D_1 = 977$ and $D_2 = 1.5$; – – –, equation (4.13) with $C_1 = 111.3$ and $C_2 = 1.0$.

Functional relationships which meet the above conditions and are consistent with the trend of the data points in figure 10 are

$$\gamma(N_P) = 1.0 + \frac{C_1}{N_P{}^{C_2}}, \tag{4.13}$$

$$\gamma(N_P) = 1.07 + \frac{D_1}{N_P{}^{D_2}}. \tag{4.14}$$

Experimental values of γ were not evaluated at the lowest of each set of data heights shown in table 1 because of the large influence at these heights of potential errors in the estimate of the buoyancy beneath them. Also the two aforementioned 'out-of-line' points in the Milgram & Van Houten data were excluded. This leaves 53 data points. C_1, C_2, D_1 and D_2 were determined so as to minimize E_γ^2, which is the square error over these 53 points:

$$E_\gamma^2 = \sum_{j=1}^{53} [\gamma_j - \gamma(N_P)]^2. \tag{4.15}$$

No weighting function of height differences was used in this case because the experimental evaluations of γ do not depend directly on measured differences at two adjacent measurement heights as was the case with α.

The values obtained for C_1, C_2, D_1 and D_2 are

$$C_1 = 337.7, \quad C_2 = 1.25, \tag{4.15a}$$

$$D_1 = 977, \quad D_2 = 1.5. \tag{4.15b}$$

Figure 10 shows these functional relationships.

$\gamma - 1$ is nearly equal to the ratio of the averages of the squared turbulent vertical velocity to the squared mean vertical velocity in a cross-section of the plume. Thus high values of γ are associated with large turbulent velocities compared with the mean, and vice versa. High values of γ have been found to occur for small values of N_P, which implies a relatively slow mean flow and relatively widely spaced bubbles. For this case much of the momentum is carried by the fluid moving with the bubbles and their distinct wakes, which is consistent with high turbulent velocities compared with the mean velocity. For large values of N_P the wakes of the bubbles are merged together, so the turbulent velocities are relatively small in comparison to the mean.

The fact that the independent variable N_P giving the best collapse of the data is a comparison of L_D with $U^2/g\Delta$ rather than $(b^2U^2/g\Delta)^{\frac{1}{3}}$ is important. If this latter characteristic length were used in forming N_P, the independent variable (cubed) would be a measure of the number of bubbles in a volume of the plume having the characteristic axial length $U^2/g\Delta$. The reason why the independent variable involves only the characteristic axial length is probably because, in general, this length is much greater than the plume radius b. As a result, the ordinary turbulence in the plume can mix the wakes of the bubbles through a lateral distance b to a much greater extent in a characteristic time $U/g\Delta$ than it can through the much larger vertical distance $U^2/g\Delta$. Thorough mixing of the wakes over this larger distance can only occur if the distance is subdivided by many bubbles, which is the case of large N_P.

4.4. *Results from other experiments*

The subsonic orifice data of Kobus (1968) and the data of Topham (1975) were analysed in precisely the same way as was done with the primary data set. Tables 3 and 4 for the Kobus and Topham data are analogous to tables 1 and 2 for the primary data set. The calculated values of α and γ for the Kobus data are also shown in figures 8–10. The γ-values for the Topham data are not reasonable. The α-values for the Topham data have unreasonable variations with height due to the irregular shapes of b *vs.* z. However, the height-averaged values of α for the Topham data are reasonable, and these are shown on figures 8 and 9.

5. Plume wandering

If a radial profile of a physical quantity in a bubble plume is measured by a set of long-term time averages, each at a radius reckoned with respect to a vertical line above the gas outlet, plume wandering can influence the measurements. In the presence of plume wandering, such a measured profile will generally have a smaller centreline value and a larger width than a profile reckoned with respect to the instantaneous location of the centreline.

5.1. *Mathematical model*

Consider a horizontal plane (X, Y) through a bubble plume whose vertical velocity profile is given by

$$u = U\exp\left(-\frac{x^2+y^2}{b^2}\right), \tag{5.1}$$

	Raw		Smooth						Airflow (normal
z	b	U	b	U	q	Q	S	γ	m³/s)
0.71	0.078	0.390	0.079	0.388	0.0003	0.007	39.86	—	
1.00	0.102	0.380	0.100	0.385	0.0003	0.012	25.98	2.78	
1.50	0.127	0.380	0.130	0.376	0.0003	0.020	15.61	2.40	
2.23	0.173	0.370	0.167	0.367	0.0003	0.032	10.09	2.19	
2.78	0.192	0.350	0.200	0.369	0.0003	0.046	7.40	1.89	0.00040
3.22	0.233	0.400	0.228	0.373	0.0004	0.061	5.86	1.64	
3.76	0.260	0.350	0.261	0.371	0.0004	0.079	4.72	1.50	
4.05	0.276	0.370	0.276	0.361	0.0004	0.086	4.38	1.53	
0.71	0.088	0.530	0.088	0.530	0.0004	0.013	39.53	—	
1.00	0.110	0.530	0.110	0.533	0.0004	0.020	25.77	1.43	
1.50	0.143	0.520	0.144	0.509	0.0004	0.033	15.86	1.28	
2.23	0.192	0.440	0.189	0.463	0.0005	0.052	10.21	1.31	
2.78	0.219	0.490	0.221	0.466	0.0005	0.071	7.79	1.19	0.00057
3.22	0.247	0.480	0.248	0.484	0.0005	0.093	6.33	1.03	
3.76	0.287	0.470	0.285	0.478	0.0005	0.122	5.07	0.94	
4.15	0.315	0.430	0.316	0.426	0.0006	0.133	4.50	1.08	
				Topham data					
5.00	1.591	1.209	1.674	1.238	0.0567	10.859	9.04	—	
14.00	3.383	1.466	3.067	1.375	0.0659	40.599	2.91	0.32	
23.00	4.013	1.191	4.444	1.266	0.0785	78.520	1.75	0.29	0.367
32.00	5.657	1.110	5.430	1.141	0.0970	105.609	1.56	0.36	
42.00	5.606	1.350	5.609	1.262	0.1316	124.681	1.85	0.40	
48.00	5.022	1.550	5.048	1.593	0.1674	127.421	2.47	0.38	
5.00	1.518	1.432	1.544	1.438	0.0685	10.724	11.55	—	
15.00	2.168	1.544	2.053	1.517	0.0809	20.036	7.44	0.64	
24.00	2.718	1.148	2.888	1.187	0.0968	31.050	5.34	0.89	0.443
34.00	4.228	0.904	4.115	0.878	0.1236	46.606	4.08	1.35	
42.70	5.307	1.061	5.339	1.068	0.1629	95.572	2.83	0.79	
4.50	1.232	1.149	1.191	1.226	0.1134	5.388	35.93	—	
7.60	1.448	1.617	1.520	1.501	0.1197	10.814	20.21	1.23	
17.00	3.012	1.545	2.948	1.570	0.1442	42.767	6.27	0.55	0.660
26.00	4.414	1.026	4.467	1.116	0.1792	69.827	4.31	0.80	
32.00	5.303	0.972	5.281	0.877	0.2138	76.660	4.29	1.29	
42.00	5.770	1.201	5.771	1.221	0.3153	127.530	4.29	0.89	

TABLE 3. The momentum-amplification factors and plume properties obtained for the Kobus and Topham data from data analysis at the measurement heights

where x and y are horizontal coordinates relative to the instantaneous centreline location. Furthermore, suppose the location of the centreline is a joint Gaussian random variable (ξ, η), whose probability density function is given by

$$p_{\xi\eta}(\xi_0, \eta_0) = \frac{1}{\pi\sigma^2}\exp\left(-\frac{\xi_0^2+\eta_0^2}{\sigma^2}\right), \tag{5.2}$$

where

$$\sigma^2 = \overline{\xi^2+\eta^2}, \tag{5.3}$$

the overbar designating the statistical average.

Let the origin of the (X, Y)-plane be at the mean centreline location, and consider measurements along $Y = 0$, which will be called u_L:

$$u_L(X) = U\exp\left(-\frac{(X-\xi_0)^2+\eta_0^2}{b^2}\right). \tag{5.4}$$

z	b	U	q	S	W	α	Airflow (normal m³/s)
			Kobus data				
0.86	0.09	0.386	0.0003	32.47	0.064	0.074	
1.25	0.12	0.381	0.0003	20.34	0.111	0.057	
1.86	0.15	0.372	0.0003	12.85	0.162	0.048	
2.51	0.18	0.368	0.0003	8.74	0.122	0.060	0.00040
3.00	0.21	0.371	0.0004	6.63	0.098	0.067	
3.49	0.24	0.372	0.0004	5.29	0.120	0.059	
3.90	0.27	0.366	0.0004	4.55	0.064	0.040	
0.86	0.10	0.531	0.0004	32.65	0.064	0.077	
1.25	0.13	0.521	0.0004	20.82	0.111	0.063	
1.86	0.17	0.486	0.0004	13.04	0.162	0.050	
2.51	0.21	0.465	0.0005	9.00	0.122	0.060	0.00057
3.00	0.23	0.475	0.0005	7.06	0.098	0.071	
3.49	0.27	0.481	0.0005	5.70	0.120	0.065	
3.95	0.30	0.452	0.0005	4.78	0.087	0.035	
			Topham data				
9.50	2.37	1.307	0.0610	5.97	0.150	0.170	
18.50	3.76	1.321	0.0716	2.33	0.150	0.135	
27.50	4.94	1.204	0.0867	1.65	0.150	0.081	0.367
37.00	5.52	1.202	0.1117	1.70	0.167	0.046	
45.00	5.33	1.428	0.1473	2.16	0.100	0.010	
10.00	1.80	1.478	0.0742	9.49	0.167	0.056	
19.50	2.47	1.352	0.0881	6.39	0.150	0.058	0.443
29.00	3.50	1.033	0.1085	4.71	0.167	0.069	
38.35	4.73	0.973	0.1405	3.46	0.145	0.195	
6.05	1.36	1.364	0.1165	28.07	0.058	0.151	
12.30	2.23	1.535	0.1308	13.24	0.177	0.158	
21.50	3.71	1.343	0.1598	5.29	0.170	0.96	0.660
29.00	4.87	0.996	0.1949	4.30	0.113	0.037	
37.00	5.53	1.049	0.2548	4.29	0.189	0.140	

TABLE 4. The entrainment coefficients and plume properties at heights midway between measurement heights for the Kobus and Topham data

The statistical average of u_L, which is representative of the long-term time average of u_L, is

$$\overline{u_L(X)} = \int_{-\infty}^{\infty}\int_{-\infty}^{\infty} u_L\, p_{\xi\eta}(\xi_0, \eta_0)\, d\xi_0\, d\eta_0. \tag{5.5}$$

Carrying out the integration results in

$$\overline{u_L(X)} = U_L \exp\left(-\frac{X^2}{b_L^2}\right), \tag{5.6}$$

where

$$U_L = \frac{U}{1+\sigma^2/b^2}, \tag{5.7}$$

$$b_L = b(1+\sigma^2/b^2)^{\frac{1}{2}}. \tag{5.8}$$

Since the plume width b at any height is a monotonically increasing function of values of the entrainment coefficient α below this height, plume wandering will result in overestimates of α if they are based on long-term time averages.

Let γ_L be the momentum-flux amplification factor based on the long-term time-average measurements U_L and b_L. Then, for the usual case of $f \ll 1$, $\rho_g \ll \rho_w$, application of (2.22) gives

$$\gamma_L = \gamma\left(1 + \frac{\sigma^2}{b^2}\right)^{\epsilon}, \tag{5.9}$$

where $1 \leqslant \epsilon \leqslant 2$ and ϵ increases with increasing $U/[u_b(1+\lambda^2)]$. Therefore, if a plume wanders, the momentum-flux amplification factor is expected to be overestimated if it is based on measurements of long-term time averages.

5.2. *Considerations of the experiments*

Fazal (1980) measured long-term time averages of momentum flux and gas fraction at an airflow rate of 0.0023 normal m^3/s in the same tank as was later used by Milgram & Van Houten (1982). The momentum-flux sensor used was subsequently found to undergo random zero shifts, so its data will not be considered here. The calibration of the gas-fraction sensor used is uncertain, so the magnitude of the gas fraction will not be considered. However, the gas-fraction profile radii, the λbs, can be compared with those later found with respect to the instantaneous centreline location to show the influence of plume wandering. These radii were determined for use here by fitting a Gaussian curve to each of the gas fraction profiles. The lowest height at which Milgram & Van Houten measured gas fractions at an airflow rate of 0.023 normal m^3/s was 1.58 m. To obtain estimates lower in the plume the value of b from the velocity data at a height of 0.96 m was multiplied by 0.8 (the estimate of λ), and the calculated result at 0.32 m (z_B) was included. Figure 11 shows the results for both the long-term time-averaged data and the data with respect to the instantaneous centreline location. The radii from the long-term time averages are clearly wider, which supports the visual observations of plume wandering in the tank and the need to measure the plume properties with respect to the instantaneous centreline location. This was done for both the Milgram & Van Houten experiments and for the larger-scale Bugg Spring experiments.

The data of Fannelop and Sjoen, which were in the form of long-term time averages, were included here in the primary data set used to determine the relationship between plume properties and α and γ. This is only justifiable if those data were not materially influenced by plume wandering. A test of this influence was provided by determining the relationship between plume properties and α and γ with the Fannelop & Sjoen data removed from the data set. There was essentially no change in the best relationship between plume properties and α. Equation (4.9) still provided the best relationship with $K = 0.165$. The only change was that the constant A changed from the value of 7.598 to 7.515. The best relationship between plume properties and γ was provided by (4.13) with $C_1 = 111.3$ and $C_2 = 1.0$. A graph of this function is shown in figure 9. The relationships between plume properties and α and γ are so little changed by exclusion of the Fannelop & Sjoen data that it is likely these data were not materially influenced by plume wandering.

The evidence concerning the influence of plume wandering on the data of Kobus (1968) is mixed. Although these data were not used in determining functional relationships between plume properties and α and γ, values of α and γ calculated from them are shown in figures 8 and 9. The values of α shown in figure 8 for the Kobus data are definitely larger than the other data and the functional relationship would predict. This indicates a possible influence by plume wandering. However, the values of γ shown in figure 9 for the Kobus data are not, for the most part, higher than other data would predict. Since this indicates a lack of influence by wandering the evidence

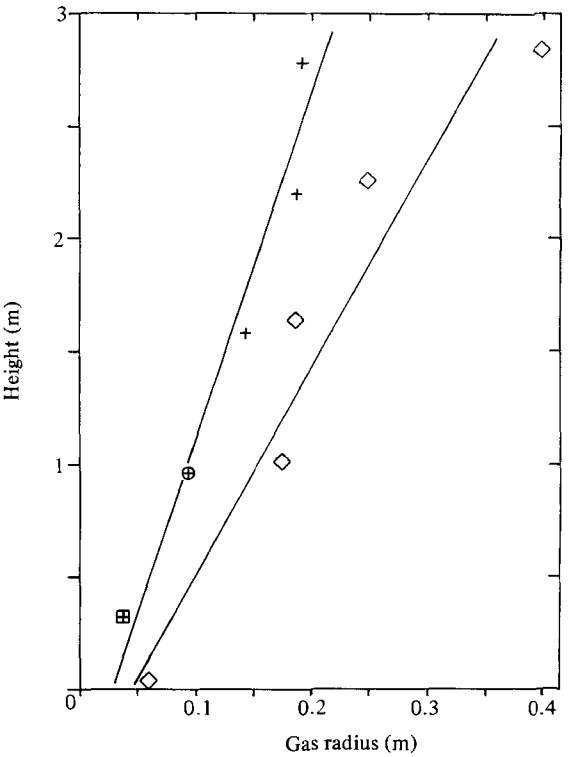

FIGURE 11. Gas radius λb *vs.* height for small-scale plumes: ◇, long-term time average measurements of Fazal; +, measurements of Milgram & Van Houten relative to instantaneous centreline, ⊕, $0.8b$ (from velocity data) for above; ⊞, $0.8 \times$ calculated value of b at z_B for above. Best straight-line fits to data (minimum mean-square error).

is mixed and no clear conclusions of the influence of wandering on the Kobus data can be drawn.

The analysis of the Bugg Spring data included determination of the location of the plume centre for each of the 60 sets of data points used in the determination of each radial profile of vertical velocity. These 60 values of centre location were used for experimental determination of σ, the variance of the radial location of the plume centre. For each height at each gasflow rate the quantity $1 + \sigma^2/b^2$ (see (5.7) and (5.8)) was determined. This quantity ranged from 1.004 to 1.092, with an average value of 1.040. This indicates that only a modest amount of plume wandering occurred in the Bugg Spring experiments, although even it was taken into account by reckoning the data with respect to the instantaneous location of the plume centreline.

6. Application

By combining the semi-empirically determined functional relations between local plume properties and the entrainment coefficient α and the momentum-amplification factor γ with the plume equations (2.15)–(2.17), numerical solutions can be obtained without the need for *a priori* specification of α and γ.

Previous experiments for determining the speed of single air bubbles in water indicate a bubble slip speed of about 0.35 m/s. Since the surface tension of natural gas against water is similar to that of air against water unless the pressure is very large, gas-bubble sizes in subsea well blowouts are expected to be similar to air-bubble

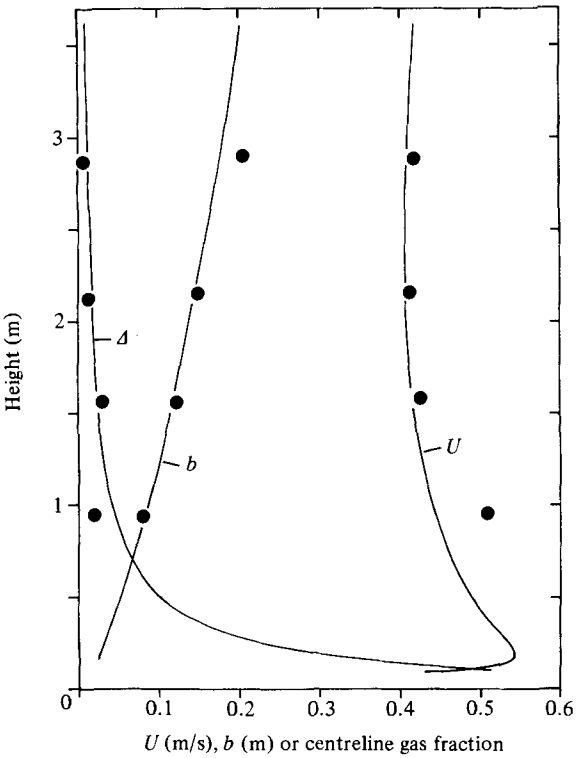

FIGURE 12. Application of the theory to the experimental conditions of Milgram & Van Houten at a gasflow rate of 0.00050 normal m^3/s: ——, numerical solution from the theory; ●, experimental value.

sizes unless the depth is very great. Bishnoi & Maini (1979) determined the downward flow speed of water required to keep natural-gas bubbles stationary in a vertical tube. These data suggest a bubble slip speed of about 0.26 m/s, but after they are corrected for tube blockage by the bubble the indicated slip speed is about 0.28 m/s. The difference in numerical results between cases with $u_b = 0.35$ and $u_b = 0.28$ is slight, and 0.35 m/s will be used for the applications here.

The gas/velocity radius ratio λ is expected to increase with increasing values of the ratio of plume velocity to slip velocity U/u_b. For relatively small plumes with $0.9 < U/u_b < 2.9$ previous measurements show $\lambda \approx 0.8$. The solution to the plume equations changes only slightly when λ changes from 0.8 to 0.9. Since λ is not expected to exceed 1.0, use of $0.8 \leqslant \lambda \leqslant 0.9$ is appropriate except for very small and slow plumes ($U/u_b < 0.5$). A value of 0.8 will be used here.

The numerical solution to the plume equations with the formulations described above for the experiment of Milgram & Van Houten (1982) at an airflow rate of 0.000 50 normal m^3/s is shown in figure 12. The measured values of U, b and centreline gas fraction are also shown in the figure. The agreement is quite good, but not as good as occurs when specific values of α and γ are chosen to give the best agreement between theory and experiment.

Figure 13 shows the numerical solution for conditions of a subsea well blowout of 10 normal m^3/s of gas at a depth of 100 m through a 0.05 m^2 opening. Although there is no quantitative data for the flow above blowouts, the results are in qualitative agreement with what is observed.

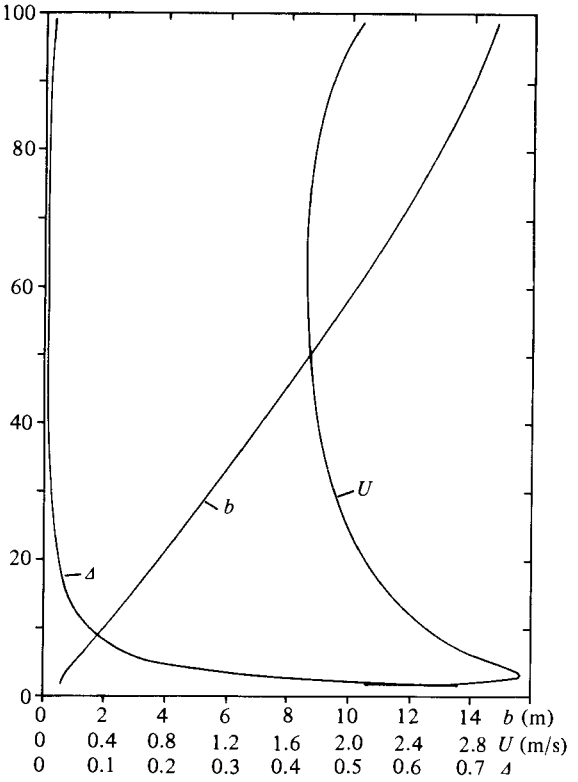

FIGURE 13. Results of numerical integration of the plume equations for a gasflow rate of 10 normal m^3/s in water that is 100 m deep.

Applications of the theory presented here are expected to be accurate for non-stratified or weakly stratified surroundings ($(U^2/g\Delta\rho_w)\,d\rho_w/dz \ll 1$). For highly stratified surroundings, McDougall (1978) has shown that a bubble plume will have a different form, because the vertical motion of fluid near the periphery of the plume is retarded and eventually stopped by its negative buoyancy.

7. Concluding discussion

The integral mean-flow plume equations (2.15)–(2.17) using Gaussian radial profiles are applicable to bubble plumes over a wide range of scales. There are four parameters in the theory: u_b, λ, α and γ. Two of them, the bubble slip speed u_b and the gas/velocity radius ratio λ, can be estimated from known information to be approximately 0.35 m/s and 0.8 respectively. Since modest changes in values of u_b or λ result in only a small change in the solution to the plume equations, these estimates can be quite approximate. Nonetheless, it would be of interest to confirm in a large-scale experiment the expectation that λ approaches 1.0 for large values of U/u_b whereas it has been found to be approximately 0.8 at small scale.

Semi-empirical functional relationships between local plume properties and the entrainment coefficient α and for the momentum-amplification factor γ have been determined. When these relationships for α and γ and the aforementioned approximations for λ and u_b are combined with the plume equations (2.15)–(2.17), the theory takes a closed form that can be applied to any round bubble plume.

The entrainment coefficient was found to increase with increasing values of the gas fraction and with increasing values of a characteristic length formed by the $\frac{4}{5}$ power

of the plume radius and the $\frac{1}{5}$ power of the mean vertical bubble speed, and to decrease with increasing values of the distance between bubbles. The combination of these effects suggests that the entrainment coefficient is increased by the mixing action of the bubbles, which increases the ratio of the r.m.s. turbulent velocity at the entrainment interface to the mean centreline velocity.

The momentum-amplification factor, which is a measure of the portion of the mean momentum flux carried by the turbulence, was found to decrease with increasing values of the characteristic vertical distance over which buoyancy causes a significant change in the momentum flux, and to increase with increasing values of the distance between bubbles. These effects are caused by the unsteadiness in the flow associated with the passage of the bubbles and their wakes. The more the relative unsteadiness, the higher the momentum-amplification factor. When there are only a few bubble spacings in the characteristic vertical distance the bubble wakes are relatively distinct, and therefore they add considerable unsteadiness to the flow. When there are many bubble spacings in the characteristic distance, the bubble wakes are more merged, so the relative unsteadiness added by the bubbles is less than in the former case.

The smallest-scale laboratory experiments that have taken place have had small enough phase distribution factors N_{P} for the momentum-flux amplification factor to be significantly greater than 1.0. However, the largest-scale laboratory experiments have had large enough phase distribution factors for γ to be nearly equal to 1.0. The available data show that γ is close to 1.0 when N_{P} exceeds 800, which would nearly always be the case for subsea well blowouts.

Small-scale laboratory tests have had considerably smaller entrainment coefficients than are expected for blowouts of gas-containing subsea wells, which result in much larger bubble Froude numbers. Available data suggest that the entrainment coefficient is relatively constant for bubble Froude numbers in excess of 50. However, very large-scale experiments are needed to confirm this.

Plume wandering was severe enough with a gas-outlet depth of 3.66 m in the 1.65 m diameter tank used by Milgram & Van Houten (1982) to necessitate special steps to measure data with respect to the instantaneous location of the moving centreline. With the exception of the mixed evidence concerning the influence of wandering on the data of Kobus (1968), wandering did not significantly influence the results of other experiments. It seems most likely that large-amplitude wandering is due to the effects of the tank walls when the horizontal extent of the facility is not very large in comparison with the plume diameter. These effects may be due to direct interaction between the plume and the sidewalls or to interactions involving the return flow in the tank. Because of the mixed evidence concerning the effects of wandering on the Kobus data, complete confirmation that large-amplitude wandering requires the influence of close sidewalls requires an experiment on small-scale plumes in a tank of large horizontal extent.

This study was supported, in part by the U.S. Department of the Interior under contract no. 14-08-001-20460, and in part by the Office of Naval Research under contract no. N00014-81-K-0785.

The efforts of Mr James J. Burgess towards construction of the current-meter array, acquisition of the data, and its reduction and curve fitting to the form of figure 6 are acknowledged and appreciated by the author. Funds for components for the current-meter array were provided by the Program for Oljevernberedskap of Norway.

REFERENCES

BISHONI, P. R. & MAINI, B. B. 1979 Laboratory study of behavior of oil and gas particles in salt water relating to deep oil well blowouts. *Spill Technology Newsletter, Environmental Protection Service, Hull, Quebec*, EPS-3-ED-80-1, 4[1], 24–36.

CHEN, C. J. & RODI, W. 1980 Vertical turbulent buoyant jets, a review of experimental data. *HMT – The Science and Application of Heat and Mass Transfer – Reports, Reviews & Computer Programs*. Pergamon.

DITMARS, J. D. & CEDERWALL, K. 1974 Analysis of air-bubble plumes. In *Proc. Coastal Engng Conf.*, chap. 128, pp. 2209–2226.

FANNELOP, T. K. & SJOEN, K. 1980 Hydrodynamics of underwater blowouts. In *Proc. AIAA 18th Aerospace Sci. Meeting, Pasadena, CA.*

FAZAL, R. 1980 Gas bubble plumes in water. MIT engineer degree thesis.

FOX, D. C. 1970 Forced plume in a stratified fluid. *J. Geophys. Res.* **75**, 6818–6835.

GEORGE, W. K. & ALPERT, R. L. & TAMANINI, F. 1977 Turbulence measurements in an axisymmetric buoyant plume. *Intl J. Heat Mass Transfer* **20**, 1145–1154.

HABERMAN, W. L. & MORTON, R. K. 1954 An experimental study of bubbles moving in liquids. *Proc. ASCE* **80**, separate no. 387.

HU, S. & KINTNER, R. C. 1955 The fall of single liquid drops through water. *AIChE J.* **1**, 42–48.

KOBUS, H. E. 1968 Analysis of the flow induced by air-bubble systems. In *Proc. Coastal Engng Conf. London*, vol. II, chap. 65, pp. 1016–1031.

MCDOUGALL, T. J. 1978 Bubble plumes in stratified environments. *J. Fluid Mech.* **85**, 665–672.

MILGRAM, J. H. & VAN HOUTEN, R. J. 1982 Plumes from sub-sea well blowouts. In *Proc. of the 3rd Intl Conf., BOSS, vol.* I, pp. 659–684.

MORTON, B. R., TAYLOR, G. I. & TURNER, J. S. 1956 Turbulent gravitational convection from maintained and instantaneous sources. *Proc. R. Soc. Lond.* **A234**, 1–23.

SEBAN, R. A. & BEHNIA, M. M. 1976 Turbulent buoyant jets in unstratified surroundings. *Intl J. Heat Mass Transfer* **19**, 1197–1204.

SJOEN, K. 1982 Data from measurements in bubble plumes. *SINTEF Project Memo., Project* no. 150030, Memo no. 1.

TOPHAM, D. R. 1975 Hydrodynamics of an oil well blowout. *Beaufort Sea Tech. Rep., Inst. Ocean Sci., Sidney, B.C.*, no. 33.

TOWNSEND, A. A. 1976 *The Structure of Turbulent Shear Flow*, 2nd edn. Cambridge University Press.